

LEVEL II

12

NAI Memorandum Report 4619

1086

**On Electron Beam Ionization of
Air and Chemical Reactions for
Disturbed Air Deionization**

A. W. Ali

Plasma Physics Division

September 22, 1981

This report was sponsored by the Advanced Research Projects Agency (DoD), DARPA Order No. 3718,
monitored by C.M. Huddleston under Contract No. N60921-80-WR-W0190.



NAVAL RESEARCH LABORATORY
Washington, D.C.

**DTIC
ELECTE
SEP 24 1981**

Approved for public release; distribution unlimited.

NAVY FILE COPY

01920172

CONTENTS

1. INTRODUCTION 1

2. ELECTRON BEAM GENERATED IONIZATION IN AIR 1

3. DEIONIZATION IN AIR WITH WATER VAPOR 15

4. REACTION RATES AND COEFFICIENTS 16

5. COMMENTS ON THE REACTION RATES AND SOME RECOMMENDATIONS.. 30

REFERENCES 33

Accession For	
NTIS GRA&I	<input checked="" type="checkbox"/>
DTIC TAB	<input type="checkbox"/>
Unannounced	<input type="checkbox"/>
Justification	
By _____	
Distribution/	
Availability Codes	
Dist	Avail and/or Special
A	

DTIC
SELECTE
 SEP 24 1981
S **D**
D

ON ELECTRON BEAM IONIZATION OF AIR AND CHEMICAL REACTIONS FOR DISTURBED AIR DEIONIZATION

1. INTRODUCTION

When a pulsed high energy electron beam propagates in the atmosphere, it loses energy through several physical processes. The energy lost by the beam is absorbed by the air molecules resulting in a certain degree of heating and ionization of the atmosphere. The degree of heating and ionization depends on the amount of energy deposited in the atmosphere by the electron beam.

The heated and the partially ionized atmosphere (disturbed air) will tend to relax to its ambient condition after the passage of the electron beam. The relaxation and the deionization of a disturbed air proceed through a host of atomic, molecular and chemical processes.

This report will deal with the generation of the disturbed air and its subsequent relaxation. It describes methods for detailed treatment of the energy deposition, the deionization processes and the air chemistry to describe the conductivity of an ionized air. The report also treats the role of water vapor on the air chemistry and reviews in detail the current status of the reaction rates pertinent to the modeling and the understanding of the deionization phenomena in air.

The electron energy deposition in air clearly will generate a plasma where a large number of plasma processes will also occur. However, this report will deal with the electron beam interaction with air purely from the point of view of the basic atomic, molecular and chemical reactions and their role on the ionization and deionization in general.

2. ELECTRON BEAM GENERATED IONIZATION IN AIR

We consider high energy ($E \geq 1$ MeV) and high current ($I \geq 1$ kA) pulsed electron beams propagating in the atmosphere. These beam electrons lose energy by three distinct processes which result in the ionization of the air species. The energy loss processes are; the inelastic collisions, the Bremsstrahlung radiation and the ohmic heating, which require distinct energy deposition treatments to calculate their contributions to the total ionization in air.

In this section, the electron beam energy loss processes will be discussed briefly along with the energy deposition methods which can be used to calculate the ionization.

2.1 ENERGY LOSS BY COLLISIONS

The primary electrons (beam electrons) lose energy by inelastic collisions with air molecules. The lost energy is expended in excitations, dissociations, ionizations of the air species and the generation of the secondary electrons. The energetic secondary electrons undergo the same energy loss processes and hence contribute to the total collisional ionization.

The energy loss per unit path, dE/dx , by relativistic electrons due to collisions with neutral species of density N can be expressed as¹

$$\left(\frac{dE}{dx}\right)_c = \frac{2\pi N e^4}{mv^2} Z \left[\log \frac{mv^2 T}{2 I^2 (1 - \beta^2)} - \left(2 \sqrt{1 - \beta^2} - 1 + \beta^2 \right) \log 2 + 1 - \beta^2 + 1/8 \left(1 - \sqrt{1 - \beta^2} \right)^2 \right] \quad (1)$$

where E is the total energy of the electron, T is its kinetic energy, $\beta = v/c$, v is the velocity of the electron, Z is the nuclear charge of the scattering atom and I is the mean excitation energy of the atom, while the rest of the symbols have their usual meanings. Equation (1) can be expressed as:

$$\left(\frac{dE}{dx}\right)_c = 4.93 \times 10^{-25} \text{ mc}^2 N Z \frac{\gamma^2}{\gamma^2 - 1} \left[\log \frac{(\gamma - 1)^2 (\gamma + 1) (\text{mc}^2)^2}{2 I^2} - (2\gamma - 1) \log 2 + \frac{(\gamma - 1)^2}{\gamma^2} \right] \quad (2)$$

where γ is the relativistic factor ($E = \gamma mc^2$). For relativistic electrons in air, at the sea level, the energy loss per unit path in units of eV, is

$$\left. \frac{dE}{dx} \right)_c = 97.33 \frac{\gamma^2}{\gamma^2 - 1} \left[\log \left\{ 1.47 \times 10^7 (\gamma - 1)^2 (\gamma + 1) \right\} - \frac{(2\gamma - 1)}{\gamma^2} \log 2 + \frac{1}{\gamma^2} + \frac{(\gamma - 1)^2}{\gamma^2} \right] \quad (3)$$

where $Z = 7.2$ and $I = 94 \text{ eV}^{1,2}$ were utilized in Equation (2). For highly relativistic electrons the first term in the bracket in Equations (1) to (3) is the dominant term and it suffices to use this term alone for the purposes of calculations. In Figure 1 we show the energy loss due to collisions by electrons in air at the sea level using Equation (3). However, it should be noted that Equations (1) - (3) do not include the density effect or what is generally called the polarization effect. The inclusion of this effect which could be calculated,³ would result in reducing the energy loss per unit path. Obviously, the polarization effect becomes appreciable^{4,5} starting with electrons with energy of 20 MeV and higher. The energy loss by collision with polarization effect included, is also shown in Figure 1 where data for $E \leq 100 \text{ MeV}$ and lower are taken from Reference 4.

Some of the features of the energy loss through collisions can be seen from Figure 1, where the energy loss decreases sharply with increasing energy until it reaches a minimum where $E \approx 2 \text{ MeV}$, then starts to rise, but slowly (logarithmically), with increasing energy. The polarization correction makes the energy loss by collisions almost a constant beyond $E \geq 200 \text{ MeV}$.

2.2 ENERGY LOSS BY RADIATION

High energy electrons lose their energy also by radiation as they traverse a gaseous medium or a material target. The radiative energy loss is due to the interaction of the incident electron with the Coulomb fields of the nucleus and the atomic electrons. The acceleration and deceleration effects on the incident electron result in Bremsstrahlung radiation. The electron energy loss by radiation, in air, becomes appreciable when $E \geq 40 \text{ MeV}$ and rises sharply with increasing electron energy (see Figure 1), and

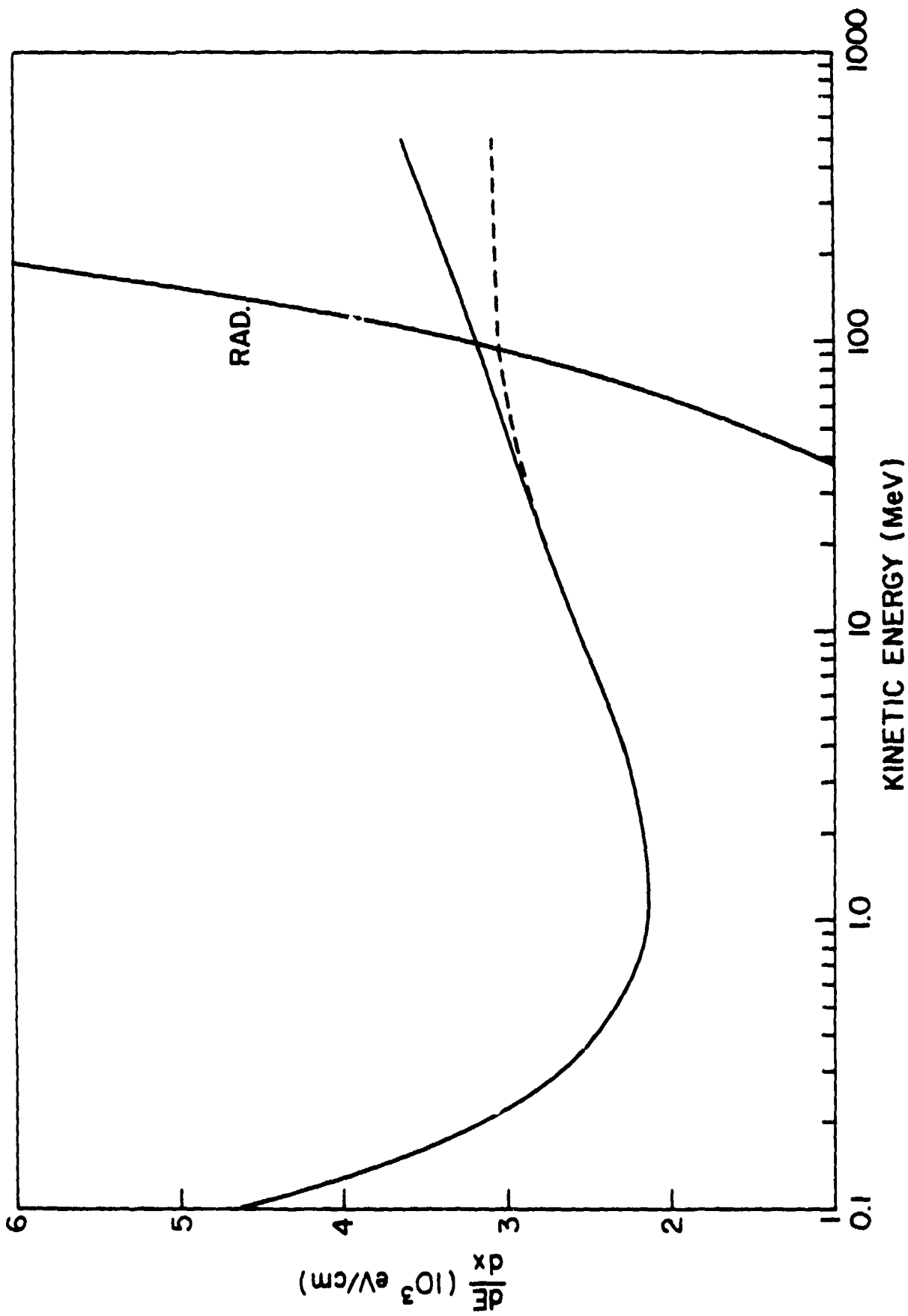


Fig. 1 - Electron energy loss per unit path in air as a function of the electron energy

becomes the dominant energy loss process for highly relativistic electrons when ≥ 200 MeV.

The energy loss by radiation for a relativistic electron with energy E is¹

$$\frac{dE}{dx}_r = N \int_0^{\nu_0} h\nu \phi(E, \nu) d\nu \quad (4)$$

where ν is the frequency of the emitted radiation and ν_0 is the upper limit for the radiated frequency defined as $E = h\nu_0 + mc^2$ and $\phi(E, \nu) d\nu$ is the cross section for the production of a photon with frequency ν in the range of $\nu + d\nu$. These cross sections have been calculated by Bethe and Heitler (see reference 1) and are given over a wide range of the screening parameter.^{1,6} As an example for complete screening^{1,6} (extremely relativistic electrons), the Bremsstrahlung radiation production cross section is^{1,6}

$$\phi(E, \nu) d\nu = \frac{Z(Z+1)}{137} (r_0)^2 \frac{d\nu}{\nu} 4 \left\{ \left[1 + \left(\frac{E - h\nu}{E} \right)^2 - \frac{2(E - h\nu)}{E} \right] \log \frac{183}{Z} + \frac{1}{9} \frac{E - h\nu}{E} \right\} \quad (5)$$

where r_0 is the electron radius. Using Equation (5) into Equation (4) and performing the integration, one obtains

$$\left(\frac{dE}{dx} \right)_r = 5.7 \times 10^{-28} Z(Z+1) N \left[4 \log \frac{183}{Z} + \frac{2}{9} \right] E \quad (6)$$

which can be written as

$$\left. \frac{dE}{dx} \right)_r = \frac{E}{L_r} \quad (7)$$

where, the radiation length, L_r , is defined as

$$L_r^{-1} = 5.7 \times 10^{-28} (Z^2 + Z) N \left[4 \log \frac{183}{Z} + \frac{2}{9} \right] \quad (8)$$

For highly relativistic electrons, the radiation length in air, at the sea level, is 300 meters. This implies that the highly relativistic electrons traversing 300 meters of air at the sea level will have their energies reduced to $1/e$ of their original value; the loss being due entirely to radiative emission, i.e. Bremsstrahlung. The energy loss per unit length (eV/cm) by the relativistic electrons in air, at the sea level is shown in Figure 1, where Equation (6) is utilized with $E \geq 100$ MeV. For $E < 100$ MeV, the $\left. \frac{dE}{dx} \right)_r$ values are taken from Reference 4.

2.3 ENERGY LOSS BY OHMIC HEATING

In addition to the energy loss by inelastic collisions and Bremsstrahlung radiation, the relativistic beam electrons lose energy through the ohmic heating of the plasma electrons. The plasma electrons gain energy from the beam induced electric field which drives a return current. The enhancement in the plasma electron energy leads to the avalanche ionization⁷ of air, especially under reduced air density conditions. When the air density is low (few Torr and lower) additional processes such as the two stream instability,^{8,9} will contribute to the generation of the plasma electrons and hence act as another mechanism for the energy loss by the beam.

The generation of the plasma electrons by collisional and other means results in an air plasma with conductivity σ given by

$$\sigma = \frac{e^2 N_e}{m \nu_m} \quad (9)$$

where ν_{in} is the momentum transfer collision frequency which includes electron-neutral and electron-ion collisions.

When the beam radial electric field is much less^{10,11} than the axial electric field, E_z , the return current density, J_z , is related to E_z by

$$j_z = \sigma E_z \quad (10)$$

To drive the return current, the beam electrons lose energy by ohmic heating. The energy lost per unit length, assuming a uniform current density, is

$$\left(\frac{dE}{dx} \right)_{ohm} = A \int_0^t j_z E_z dt \quad (11)$$

where A is the beam area cross section. The parameters σ , j_z and E_z in Equation (11) can be obtained using the appropriate rate equations to calculate σ and the usual circuit equations¹⁰ for the current driven by the electron beams. However, an estimate can be made for the energy loss, due to ohmic heating. Using a one dimensional circuit equation, assuming a fast current rise time and beam pulses short enough so that I_n is roughly constant, one obtains,

$$\left(\frac{dE}{dx} \right)_{ohm} \approx L I_b I_n \quad (12)$$

where L is the circuit inductance per unit length, I_b and I_n are the beam and net currents, respectively.

2.4 IONIZATION CALCULATION

In this section we discuss methods for the ionization calculations due to the energy loss processes presented in Sections 2.1 - 2.3.

The collisional ionization consists of the direct ionization by the beam electrons (primary electrons) and the ionization by the secondary electrons generated by the act of the primary ionization. One of the often

used concepts for the collisional ionization calculation is the method of the continuous slowing down approximation.¹²⁻¹⁴ In this method one calculates the primary ionization, obtains the secondary and the tertiary electron distribution and their contributions to the total collisional ionization. It has been utilized¹⁴⁻¹⁸ for electron and proton depositions in N_2 , O_2 and O in the upper atmosphere for the understanding of the auroral phenomenon. This energy deposition concept has been improved to include discrete energy depositions for electrons with energy below 500 eV and has been applied to auroral phenomenon^{17,18} as well as depositions in other gaseous elements.¹⁹⁻²¹ Such a treatment of a detailed energy deposition is in progress at NRL. It requires a large number of ionization and excitation cross sections and has the advantage of providing excitation rates to all electronic states, for a detailed air chemistry and plasma emission calculations. Some of these electronic states, with radiation emissions in the optical region, can be utilized for various beam diagnostic purposes.

The ionization of air by the Bremsstrahlung radiation is more complicated and depends on the flux and the energy distribution of the emitted photons. These photons, absorbed and scattered by the air molecules, generate free electrons by (a) photoabsorption, (b) Compton effect and (c) pair production. The free electrons generated in this manner deposit their energies collisionally as well as by radiative losses. Thus, the Bremsstrahlung ionization of air can be described and calculated as a cascade shower^{5,22} ionization.

A detailed Bremsstrahlung energy deposition in air is accomplished by the calculation of the flux and the energy distribution of the emitted photons for each primary electron. These photons then are deposited in air as a function of distance using the cross sections for the ionization of air due to the photoabsorption, Compton effect and pair production. These cross sections, shown in Figure 2 in the form of the attenuation coefficient,²³ μ , ($\mu = \sum_1 \mu_1$, $\mu_1 = \sigma_1 N_1$) indicate the role of each process, in air, as a function of the radiation wavelength. For each process, the energy of the ejected electron is calculated and its energy is deposited according to the energy loss processes. Such an energy deposition for the Bremsstrahlung radiation is under consideration at NRL.

The calculation of the beam energy loss by ohmic heating can be carried out also in detail by solving Maxwell's equations, the kinetic equations and

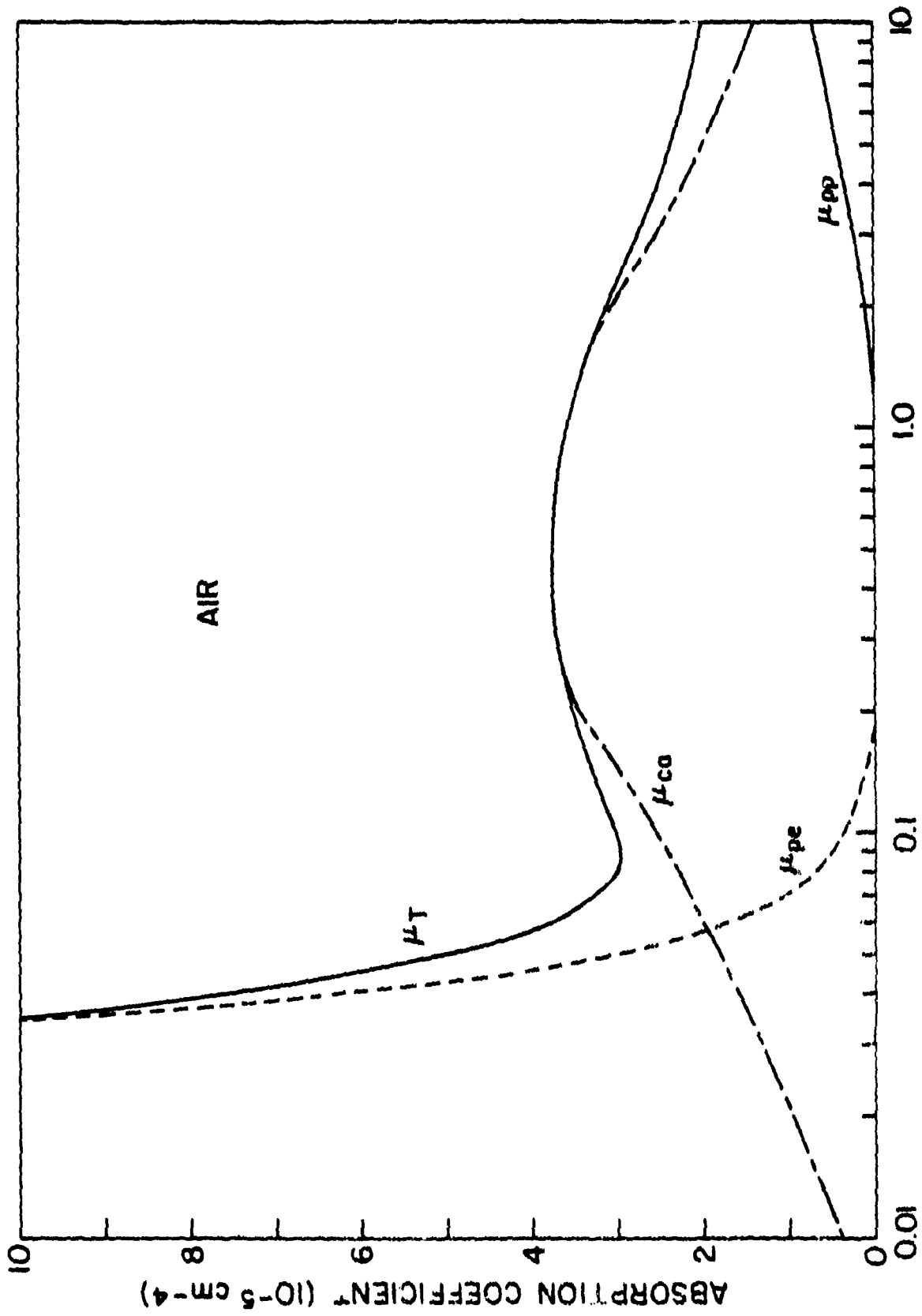


Fig. 2 - The absorption coefficient of radiation in air

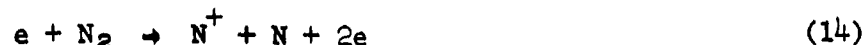
the appropriate circuit equation to calculate various currents (I_n , I_p , etc.) and the air conductivity.

These energy deposition schemes described, briefly, to account for the ionization in air were described separately. In reality, however, the energy loss processes are simultaneous occurrences, albeit one more important than the other at different times, pressures, and positions of interest. Furthermore, good estimates for ionization can be obtained using simpler methods e.g. the energy per ion pair generation concept for the collisional and radiative losses and using a simple circuit equation^{1,2} to describe the ohmic heating.

3.0 THE IONIZATION AND THE DEIONIZATION PROCESSES IN AIR

In this section, we give an overview of the ionization and the deionization processes, in air, which occur during the passage of a pulsed relativistic electron beam. The purpose of this overview is to provide the understanding of the patterns of the charge flow and how they control the time history of the electron density and consequently the air conductivity.

The ionization in the ambient air proceeds by electron impact on the air molecules and by their absorption of radiation. The collisional ionization produces air species ions in the form of N_2^+ , N^+ , O_2^+ and O^+ . These ions are formed by two distinct processes, which are the ionization and the dissociative ionization of the air molecules, as described by Equations 13-16.



The ionization resulting from the absorption of radiation proceeds by photoionization and by collisional ionization, where the last process is due to the Compton and the pair produced electrons. For photons with low energies ($h\nu \approx 15 - 200$ eV), the ionization proceeds by the ionization of the valence electrons as described in Equations 17 - 20





However, for photons with energies above 200 eV and where Compton effect is small the photoionization proceeds via the inner shell ionization and one generates N_2^{++} and O_2^{++} due to the Auger process²⁴ because the x-ray fluorescence yield²⁵ is very low for low z elements. These doubly ionized molecules, however, will be converted to $2 N_2^+$ and $2 O_2^+$ through charge exchange with their respective molecules.

The oxygen and nitrogen atoms are also generated by the electron impact dissociations of N_2 and O_2



and by the dissociative recombinations of the molecular ions

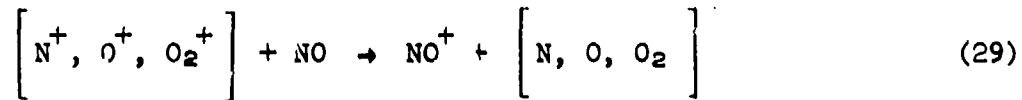


Since these processes (i.e. Reactions 21-25) occur during the electron beam pulse, the atomic species are ionized by electron impact to also produce the ionic species of N^+ and O^+ . The nitric oxide, NO, is produced mainly by



The NO^+ ion, however, is produced by electron impact and photoionization of NO, by charge exchange and by ion-molecule rearrangement processes which are

described below.



The deionization of the air plasma occurs during the passage of the electron beam and continues afterwards, until the free electrons, the positive ions and the negative ions have disappeared completely.

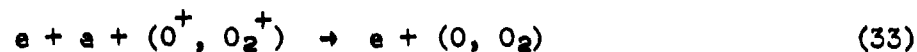
The deionization proceeds as follows; the electrons disappear in two ways (1) by recombinations with the ions, (2) by attachment and dissociative attachments to molecules. The attachments generate negative ions which deplete the positive ion concentrations by mutual neutralization (ion-ion recombination). However, during the deionization the positive ions undergo a multitude of reactions, such as charge exchange, ion-molecule rearrangements and associations. These processes are important because generally they convert an atomic ion into a molecular one or a molecular ion into a cluster ion, thereby speeding up the plasma recombinations. This is because the molecular and cluster ions recombine faster with electrons compared to the recombination of electrons with atomic ions, especially for air plasmas with $N_e < 4 \times 10^{16} \text{ cm}^{-3}$.

To illustrate the deionization processes in air, the molecular ions N_2^+ and O_2^+ recombine dissociatively with the plasma electrons i.e.

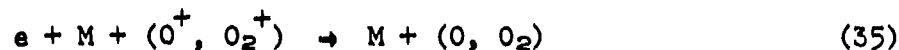
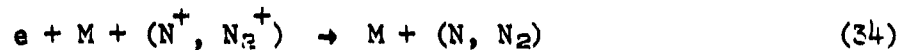


These ions, also undergo collisional-radiative recombination along with atomic ions. However, for regions of interest we can ignore the radiative recombination and consider only the three-body (collisional) recombination, e.g.





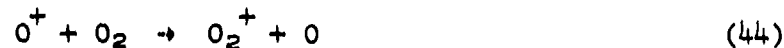
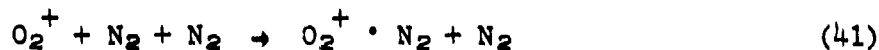
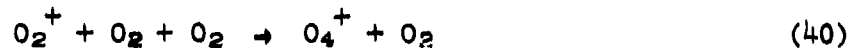
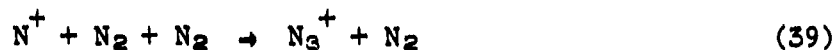
Three-body recombination also proceeds with the third body being a neutral species, e.g.,



Apart from these direct paths which deplete the free electron concentration, the free electrons and the atmospheric ions follow different paths. The free electrons are lost by three-body and dissociative attachments with O_2 , whereupon stable negative ions are generated, e.g.,



The positive ions, however, undergo clustering, charge exchange and ion atom interchange processes which are

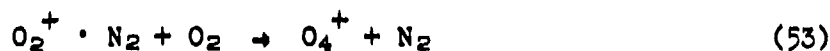
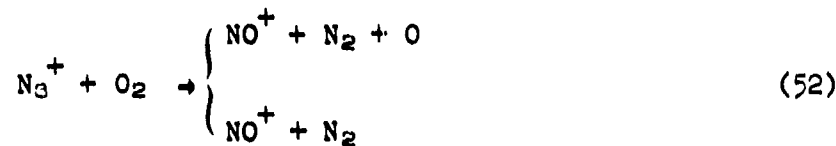


The clustered ions will recombine with the free electrons via dissociative recombinations e.g.



and by three-body recombinations (see Reactions 32-35).

These clusters, however, undergo charge exchange, rearrangement and switching processes



It is obvious from reactions 42-46, 51 and 52 that there are various charge exchange and ion atom rearrangements which proceed to produce O_2^+ and NO^+ , where the last ion recombines dissociatively with the plasma electrons (see Reaction 25) and by various three-body recombinations (see Reaction 32-35). Finally, the mutual neutralization of the positive and the negative ions can proceed via two and three body processes. The former is represented by the following reactions



where A^+ , A_2^+ and A_n^+ are atomic, molecular and cluster ions, respectively. For the three-body neutralization add M to both sides of equations 54 and 55.

However, when air is moist and contains some amount of H_2O , the deionization becomes more complicated as discussed in the next section.

3. DEIONIZATION IN AIR WITH WATER VAPOR

The presence of water vapor in air adds additional complication to the deionization of the disturbed air. Various positive clustered ions are formed with the terminal ion being a hydrated hydronium, $H_3O^+ \cdot (H_2O)_n$. These ions have been observed by Narcisi and Bailey²⁶ and the reactions leading to the generation of these hydrates starts with O_2^+ as a precursor ion and is well understood.^{27, 28} These hydrates are also generated starting with the hydration of NO^+ .

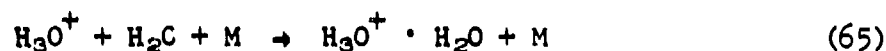
The pertinent reactions which lead to the generation of various hydrated ions can be summed as follows. The positive ions N^+ , N_2^+ , N_3^+ , N_4^+ and O^+ react with H_2O according to the following reactions.



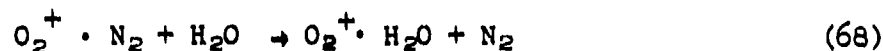
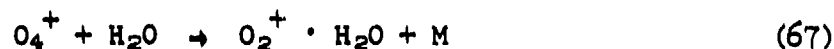
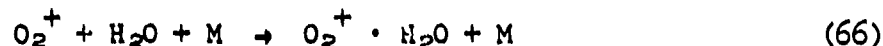
Reactions (56) through (61) obviously produce predominantly H_2O^+ which in turn undergoes the following reactions



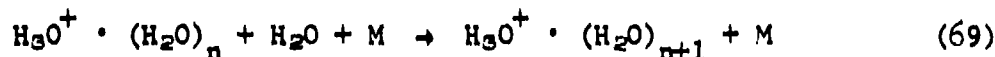
Reaction (64) generates the hydronium, H_3O^+ , which in turn generates the hydrated hydronium according to



The following reactions, an association and two switching, result in the production of $\text{O}_2^+ \cdot \text{H}_2\text{O}$



On the other hand, $\text{O}_2^+ \cdot \text{H}_2\text{O}$ reacts with H_2O to produce $\text{H}_3\text{O}^+ \cdot \text{OH}$ which in turn produces $\text{H}_3\text{O}^+ \cdot \text{H}_2\text{O}$ through a switching reaction with H_2O . This indicates two routes for the production of $\text{H}_3\text{O}^+ \cdot \text{H}_2\text{O}$, one initiated by H_3O^+ , and the other by $\text{O}_2^+ \cdot \text{H}_2\text{O}$ where O_2^+ and O_4^+ are precursor ions. Other hydrates are generated according to



All these new clusters recombine with the free electrons through the dissociative recombination and mutual neutralization process to produce neutral products.

As for the impact of water vapor on negative ions, the attachment of the free electrons to O_2 proceeds as in Equation (36) with $\text{M} = \text{H}_2\text{O}$.

The negative ions also generate their own ion clusters in the form of NO_3^- , CO_3^- , etc., which are subsequently converted into hydrated negative ions.

4. REACTION RATES AND COEFFICIENTS

To calculate the air plasma conductivity, a time dependent model for the electron energy deposition coupled to a detailed air chemistry code is required. The electron energy deposition, however, requires a large set of inelastic cross sections for electron collision with the air species. A set of cross sections appropriate to this problem is reported elsewhere.²⁹

A detailed air chemistry code, however, requires the appropriate reaction rates which determine the time history of each species. Furthermore, one

requires the calculation of the plasma electron temperature, the gas kinetic temperature, assuming the ions and neutrals to have the same temperature, and vibrational temperature of the molecules. This is essential because the various reaction rates presented in the preceding sections depend on these temperatures.

In this section we review the pertinent reaction rates, coefficients and their temperature dependence in order to delineate their utility for the modeling of the air plasma. It is obvious that many of these coefficients are known over a limited range of temperatures and their extension to higher temperatures may not be accurate.

4.1 THE DISSOCIATIVE RECOMBINATION OF AIR IONS

The dissociative recombination rate coefficients of N_2^+ , O_2^+ and NO^+ have been measured under several distinct and different experimental methods. These are, the afterglow,^{30, 31} the ion storage³² and the merged electron-ion beam experiments.³³ These different techniques yield results in good agreement for the dissociative recombination of O_2^+ . They predict^{30, 32, 33} an electron temperature dependent rate coefficient which varies as $T_e^{-0.5}$ for an electron temperature from 0.1 to 1.0 eV.

For NO^+ , however, the agreement on the measured³¹⁻³³ dissociative recombination rate coefficient and its dependence on the electron temperature is not satisfactory. For example, the afterglow experiment³¹ yields an electron temperature dependence of $T_e^{-0.37}$ while the ion storage technique³² gives a temperature dependence of $T_e^{-0.83}$. The merged electron ion beam experiment³³ predicts a temperature dependence of $T_e^{-0.5}$. There is a reasonable agreement between the results of the ion storage technique³² and the merged electron-ion beam experiment.³³ However, these results differ by a factor of 2 to 3 from those of the afterglow measurements³¹ in the electron temperature range of 0.1-1.0 eV.

For N_2^+ , the afterglow³⁰ and the merged electron-ion beam method³³ yield, for the dissociative recombination rate coefficient, a temperature dependence of $T_e^{-0.39}$ and $T_e^{-0.5}$, respectively. The disagreement is 30% in the electron temperature range of 0.034-1.0 eV.

The disagreement in the dissociative recombination coefficients summarized in Table 1, may be due to the ions being vibrationally excited³¹ compared to those being in the ground state.³³

Table 1 The Dissociative Recombination Rate Coefficients of N_2^+ , O_2^+ and NO^+

<u>Process</u>	<u>Rate Coefficient (cm³/sec)</u> (T_e in eV)	<u>Reference</u>
$N_2^+ + e \rightarrow N + N$	$4.3 \times 10^{-8} T_e^{-0.39}$	30
	$5.5 \times 10^{-8} T_e^{-0.5}$	33
$O_2^+ + e \rightarrow O + O$	$1.5 \times 10^{-8} T_e^{-0.7}, T_e \leq 0.1$	30
	$2.1 \times 10^{-8} T_e^{-0.5}, T_e > 0.1$	
$NO^+ + e \rightarrow N + O$	$2 \times 10^{-8} T_e^{-0.83}$	32
	$9.8 \times 10^{-8} T_e^{-0.37}$	31
	$3.6 \times 10^{-8} T_e^{-0.5}$	33

4.2 DISSOCIATIVE RECOMBINATION RATE COEFFICIENTS OF AIR ION CLUSTERS (N_3^+ , N_4^+ , O_4^+ , ...)

The rate coefficient for the dissociative recombination of N_4^+ has been measured at room temperature ($T_e = T_a$) by Kasner and Biondi.³⁴ There is no temperature dependent measurement for the recombination coefficient, however, the temperature dependence has been inferred from the measurement of an effective recombination coefficient³⁵ for a pure N_2 plasma. This effective recombination, measured in the temperature range of 295 - 694°K with electrons, ions and the neutrals having the same temperature, yields a $T_a^{-1.07}$ dependence for the recombination. Since the measurement³⁵ was made at nitrogen pressures of 10 - 15 Torr, the effective recombination coefficient is in reality close to that for the recombination of N_4^+ , because N_4^+ will be the dominant ion. However, other ions such as N_2^+ and N_3^+ are also present albeit at quantities much less than that of N_4^+ . It is of interest to note, however, that the room temperature value for the effective recombination rate coefficient³⁵ is in good agreement with the dissociative recombination of N_4^+ as measured by Kasner and Biondi.³⁴

There is no measurement for the dissociative recombination of N_3^+ . It is expected, however, that the rate coefficient for its dissociative recombination to fall somewhere between those of N_2^+ and N_4^+ . An estimated value and its temperature dependence of $T_e^{-1.1 \pm 0.5}$ has been proposed by Biondi.^{36,37}

As for O_4^+ there exist two measurements for its dissociative recombination, one at a temperature of 205°K (ref. 38) and the other at 180°K (ref. 39). The extrapolation of this data to higher electron temperature is assumed to follow a $T_e^{-1.0}$ dependence in similarity to N_4^+ .

The dissociative recombination rate coefficients for the air ions are given in Table 2, where the coefficient for $O_2^+ \cdot N_2$ is only an estimate⁴⁰

Table II The Dissociative Recombination Rate Coefficients of Air Ion Clusters

<u>Reaction</u>	<u>Coefficient (cm³/sec)</u> (T_e in eV)	<u>Reference</u>
$N_4^+ + e \rightarrow N_2 + N_2$	2×10^{-8} , $T_e = 0.025$ eV	34
	$3.4 \times 10^{-8} \left(\frac{1}{T_e}\right)^{1.1}$	35
$N_3^+ + e \rightarrow N + N_2$	$1.75 \times 10^{-8} \left(\frac{1}{T_e}\right)^{1 \pm 0.5}$	36, 37
$O_4^+ + e \rightarrow O_2 + O_2$	2×10^{-8} , $T_e = 0.017$ eV	38
	$3.4 \times 10^{-8} \left(\frac{1}{T_e}\right)^{1.0}$	36, 37
	1.8×10^{-8} , $T_e = 0.015$ eV	39
$O_2^+ \cdot N_2 + e \rightarrow O_2 + N_2$	$3.7 \times 10^{-8} \left(\frac{1}{T_e}\right)^{1.0}$	40

4.3 DISSOCIATIVE RECOMBINATION OF H_3O^+ , ITS HYDRATES AND SOME PERTINENT CLUSTERS

The dissociative recombination rate coefficient of hydronium, H_3O^+ , has been measured by Leu, et al⁴¹ at a temperature of 540°K (electrons, ions and neutrals were in thermal equilibrium). Heppner, et al,⁴² have measured

the cross section for the dissociative recombination in the electron energy range of 0.06 - 1.15 eV where the gas temperature was kept at 400°K. Averaging this cross section over a Maxwellian electron velocity distribution, Heppner, et al.⁴² obtain a rate coefficient which follows a temperature dependence of $T_e^{-1.0}$ between 0.025 and 1 eV and is in good agreement with the rate proposed by Biondi.³⁶ However, the temperature dependence follows $T_e^{-1.2}$ above $T_e = 2\text{eV}$ and reaches a $T_e^{-1.43}$ dependence at $T_e = 10\text{eV}$.

In addition to the above measurements,^{41,42} the dissociative recombination of H_3O^+ has been measured extensively in flames, shock tubes, and afterflow experiments. Two previous measurements^{43,44} in the temperature range of (2000 - 2500°K) and a measurement⁴⁵ at 1000°K are in good agreement with results of Heppner, et al.⁴² Other high temperature measurements of the rate coefficient, with $T_e = T_i = T_a$ yield reasonable values, in the temperature range of 2000 - 2500°K, compared to measurements of Heppner, et al.⁴² However, the measurement of Ogram, et al.⁴⁶ yields a dependence of $T_e^{-0.5}$ for the rate coefficient in the temperature range of 0.075 to 0.77eV. This temperature dependence is similar to that obtained using the cross section measurement ($T_e \leq 0.08\text{eV}$) of McGowan et al.⁴⁷ However, they differ by more than a factor of 2 in magnitude. The summary of these rate coefficient measurements is given in Table III.

There is no measurement for the dissociative recombination of H_2O^+ in afterglow type experiment. This may primarily be due to the fast switching⁴⁸ reaction of H_2O^+ with H_2O generating H_3O^+ . However, merging beam technique⁴⁷ predicts $\sim 1/\sqrt{T_e}$ dependence for the recombination coefficient for electron temperatures of $T_e \leq 0.1\text{ eV}$.

The dissociative recombination of $\text{H}_3\text{O}^+ \cdot (\text{H}_2\text{O})$ has been measured⁴¹ at 415 and 540°K while for $\text{H}_3\text{O}^+ \cdot (\text{H}_2\text{O})_2$ the measurements are made at 300, 415 and 540°K. Those temperatures are thermal equilibrium values, where $T_e = T_a$. From these measurements the temperature dependence for these dissociative recombinations are deduced and are given in Table II. It should be noted, that the dissociative recombination of the hydrated hydronium, $\text{H}_3\text{O}^+ \cdot (\text{H}_2\text{O})_n$ have a weak or no dependence on the electron temperature, especially for $n \geq 2$.

Few other clusters of interest e.g. $\text{O}_2^+ \cdot \text{H}_2\text{O}$, and $\text{H}_3\text{O}^+ \cdot \text{OH}$ have no measured or calculated values for their recombination coefficients. However,

estimates can be given, and are presented in Table III.

Table III
The Dissociative Recombination of H_3O^+ and Some Pertinent Clusters

<u>Reaction</u>	<u>Coefficient (cm³/sec)</u> (T_e in eV)	<u>Reference</u>
$\text{H}_3\text{O}^+ + e \rightarrow \text{H} + \text{H}_2\text{O}$	$3.2 \times 10^{-7} T_e^{-1.0}$, $0.025 \leq T_e \leq 0.66$	36
	1.0×10^{-6} , $T_e = 0.046$	41
	$2.56 \times 10^{-8} (\frac{1}{T_e})^{1.2}$, $0.26 \leq T_e \leq 2.15$	42
	$3.05 \times 10^{-8} (\frac{1}{T_e})^{1.43}$, $2.15 < T_e < 8.6$	42
	6.0×10^{-7} , $T_e = 0.086$	45
	2.0×10^{-7} , $T_e = .172$	43
	$1.1 \times 10^{-8} T_e^{-0.5}$, $T_e \leq 0.08$	47
	$1.18 \times 10^{-7} T_e^{-0.5}$, $T_e \leq 0.77$	46
$\text{H}_2\text{O}^+ + e \rightarrow \text{O} + \text{H}_2$	$1.2 \times 10^{-8} (\frac{1}{T_e})^{0.5}$, $T_e \leq 0.1 \text{ eV}$	47
$\text{H}_3\text{O}^+ \cdot \text{H}_2\text{O} + e \rightarrow 2\text{H}_2\text{O} + \text{H}$	$1.6 \times 10^{-6} (\frac{1}{T_e})^{0.15}$	36, 37
$\text{H}_3\text{O}^+ \cdot (\text{H}_2\text{O})_2 + e \rightarrow 3\text{H}_2\text{O} + \text{H}$	$4.2 \times 10^{-6} (\frac{1}{T_e})^{0.05}$	36, 37
$\text{O}_2^+ \cdot \text{H}_2\text{O} + e \rightarrow \text{O}_2 + \text{H}_2\text{O}$	$7.2 \times 10^{-7} (\frac{1}{T_e})^{0.2}$	37
$\text{H}_3\text{O}^+ \cdot \text{OH} + e \rightarrow \text{H}_2\text{O} + \text{H} + \text{OH}$	$9.5 \times 10^{-7} (\frac{1}{T_e})^{0.2}$	37

4.4 POSITIVE ION-NEUTRAL ASSOCIATION

The three-body association rate coefficient of N_2^+ with 2N_2 to form N_4^+ has been measured⁴⁹⁻⁵⁹ at room temperature, 300°K and as a function of E/P (E is the electric field and P is the pressure). The most recent measurement⁵⁹ yields a rate coefficient of $5.5 \times 10^{-26} \text{ cm}^3/\text{sec}$. The temperature dependence can be inferred from the measurements of Good, et al⁵⁷ which were made at 300°K and 380°K. An 80°K rise in the gas temperature

reduces the association rate coefficient by a factor of 2.5 indicating a $T_a^{-3.9}$ dependence. A most recent measurement⁶¹ of the association coefficient with the third body being He gives a value of 1.1×10^{-29} cm³/sec. If one normalizes this value for N₂ as a third body by multiplying it by an empirical factor of 4 determined by Niles⁶¹ a value of 6×10^{-29} cm³/sec is obtained. A suggested³⁷ temperature dependence of $T_a^{-1.0}$ has been given with an uncertainty in the temperature exponent of (+1 to -2.0).

The three-body association rate coefficient of N⁺ with 2N₂ to form N₃⁺ has been measured^{57,59,63} at room temperature, with the recent value⁵⁹ being 2.7×10^{-29} cm³/sec compared to 5.0×10^{-29} cm³/sec (ref. 57) and 1.8×10^{-29} cm³/sec (ref. 63). A recent measurement⁶¹ of the association coefficient with the third body being He gives a room temperature value of 5.2×10^{-30} cm³/sec. If one utilizes the empirical factor⁶² of 4 to convert the coefficient from He to nitrogen as a third body, one obtains a value of 2.1×10^{-29} cm³/sec, suggesting that the recent measurement⁵⁹ to be a best value. There exists, however, no measurement at temperatures above 300°K. Thus, the temperature dependence for the association of N⁺ to form N₃⁺ is only estimated.³⁷

The three-body association rate coefficient of O₂⁺ with 2O₂ to form O₄⁺ has been measured⁶⁴ at room temperature and as a function⁶⁵ of gas temperature (between 80°K and 300°K). The room temperature rate coefficient is 2.5×10^{-30} cm³/sec and the temperature dependence inferred from this limited range follows $T_a^{-3.2}$. The association of O₂⁺ with 2N₂ to form O₂⁺ · N₂ has an estimated³⁷ rate coefficient.

The association of O₂⁺ with H₂O to form O₂⁺ · H₂O with the third body being N₂ and O₂ has been measured^{64,66} and the corresponding rate coefficients at T_a = 300°K are 2.8×10^{-29} cm³/sec and 2.3×10^{-29} cm³/sec, respectively. The temperature dependence of this coefficient is estimated.³⁷

The three-body association of hydronium to form the first hydrated hydronium has been measured^{63,65} with the third body being N₂ and O₂. The room temperature coefficients are 3.4×10^{-27} cm³/sec and 3.7×10^{-27} cm³/sec for M = N₂ and M = O₂, respectively. However, the temperature dependence of the association is estimated.³⁷

The three-body association of H₃O⁺ · H₂O with H₂O to form H₃O⁺ · (H₂O)₂ has also been measured⁵⁷ with the third-body being N₂ and O₂. The room

temperature coefficients are 2.3×10^{-27} cm³/sec and 2.0×10^{-27} cm³/sec for M = N₂ and M = O₂, respectively. The temperature dependence, however is estimated.³⁷ The rate coefficients described in this section are summarized in Table IV.

Table IV
Positive Ion-Neutral Association Coefficients

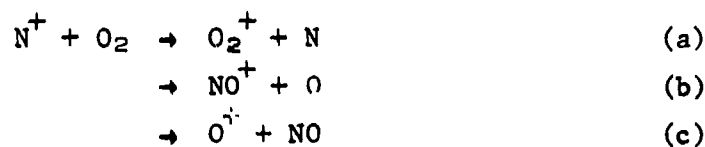
<u>Reaction</u>	<u>Coefficient (cm³/sec)</u>	<u>Reference</u>
N ₂ ⁺ + 2N ₂ → N ₄ ⁺ + N ₂	$5.5 \times 10^{-27}, T_a = 0.025$	59
	$8.0 \times 10^{-29}, T_a = 0.025$	57
	$3.2 \times 10^{-29}, T_a = 0.031$	57
	$6.0 \times 10^{-30}, T_a = 0.025$	60
	$1.7 \times 10^{-29}, M = \text{He}$	61
	$3.1 \times 10^{-35}, \left(\frac{1}{T_a}\right)^{3.9}$	57, 59
N ⁺ + 2N ₂ → N ₃ ⁺ + N ₂	$1.3 \times 10^{-30}, \left(\frac{1}{T_a}\right)^{1.0 \pm 1.0}$	37
	$2.7 \times 10^{-29}, T_a = 0.025$	59
	$1.8 \times 10^{-29}, T_a = 0.025$	63
O ₂ ⁺ + 2O ₂ → O ₄ ⁺ + O ₂	$5.2 \times 10^{-30}, M = \text{He}$	61
	$2.1 \times 10^{-29}, M = \text{N}_2$	see text
	$2.5 \times 10^{-30}, T_a = 0.025$	64
	$1.94 \times 10^{-35}, \left(\frac{1}{T_a}\right)^{3.2}$	35
O ₂ ⁺ + M + H ₂ O → O ₂ ⁺ · H ₂ O + M	$3.8 \times 10^{-35}, \left(\frac{1}{T_a}\right)^{3.2}, M = \text{N}_2$	37
	$2.8 \times 10^{-29}, M = \text{N}_2, T_a = 0.025$	64, 66
	$2.3 \times 10^{-29}, M = \text{O}_2, T_a = 0.025$	64
	$1.75 \times 10^{-31}, \left(\frac{1}{T_a}\right)^{2.0}, M = \text{N}_2$	37

Table IV continued

<u>Reaction</u>	<u>Coefficient</u>	<u>Reference</u>
	$1.43 \times 10^{-31} \left(\frac{1}{T_a}\right)^{2.0}, M = O_2$	37
$O_2^+ + N_2 + N_2 \rightarrow O_2^+ \cdot N_2 + N_2$	$5.6 \times 10^{-34} (T_a)^{-2.0}$	37
$H_3O^+ + H_2O + M \rightarrow H_3O^+ \cdot H_2O + M$	$3.4 \times 10^{-27}, T_a = 0.025, M = N_2$	57
	$3.7 \times 10^{-27}, T_a = 0.025, M = O_2$	57
	$2.1 \times 10^{-30} (T_a)^{-2.0}, M = N_2$	37
	$1.4 \times 10^{-33} (T_a)^{-4.0}, M = O_2$	37
$H_3O^+ \cdot H_2O + H_2O + M \rightarrow$ $H_3O^+ \cdot (H_2O)_2 + M$	$2.3 \times 10^{-27}, M = N_2, T_a = 0.025$	57
	$2.0 \times 10^{-27}, M = O_2, T_a = 0.025$	57
	$1.4 \times 10^{-30} \left(\frac{1}{T_a}\right)^{2.0}, M = N_2$	37
	$7.8 \times 10^{-33} \left(\frac{1}{T_a}\right)^{4.0}$	37

4.5 CHARGE EXCHANGE, SWITCHING AND REARRANGEMENT REACTIONS

The reaction of N^+ with O_2 has three outgoing channels, i.e.



The overall reaction rate has been measured at room temperature by McFarland, et al,⁶⁷ Smith, et al,⁶¹ and McCrumb and Warneck.⁵⁹ The corresponding measurements yield 5.5×10^{-10} , 6.1×10^{-10} and 7.5×10^{-10} in units of cm^3/sec , respectively. The branching ratios have also been measured with agreement within 10% for reactions a and b and 30% for reaction c. The measured temperature dependence of the overall rate coefficient yields⁶⁷ no apparent dependence on temperature up to $T_i = 0.39eV$. However, above $T_i = 0.39eV$ the temperature dependence follows $T_i^{0.57}$. Thus, one can utilize the overall reaction rate and the branching ratio as measured by Smith, et al⁶¹, coupled to the temperature dependence obtained by McFarland, et al⁶⁷ to obtain the

the best rates for these reactions.

The rate coefficient for the charge exchange of N_2^+ with O_2 has been measured at room temperature^{61,67} and as a function of the ion temperature.⁶⁷ The room temperature values of reference 61 and 67 are 5.1×10^{-11} cm³/sec and 5.0×10^{-11} cm³/sec, respectively.

The reaction of N_3^+ with O_2 resulting in two channels which produce NO^+ and NO_2^+ , have been measured at room temperature.^{59,61,68} The temperature dependence of the coefficient for the overall reaction has also been measured⁶⁷ in the temperature range of 0.025eV to 0.075eV. The overall room temperature values are 7.7×10^{-11} cm³/sec, 5.1×10^{-11} cm³/sec and 6×10^{-11} cm³/sec as obtained by references 59, 61 and 68, respectively.

The rate coefficient for the charge exchange of N_4^+ with O_2 has been measured at room temperature^{59,61} and as a function⁶⁹ of the ion energy in the range of 0.04 to 0.2eV ($T_1 \approx 0.025 - 0.132$ eV). The room temperature values of the coefficient are 4×10^{-10} cm³/sec, 2.5×10^{-10} and 2.5×10^{-10} cm³/sec, as obtained by references 59, 61 and 69, respectively. No temperature dependence has been observed for the ion temperature from 0.025 eV to 0.0132 eV.

The rate coefficient for the charge exchange of O^+ with O_2 have been measured at room temperature^{61,67,70} and as a function of the ion temperature.^{67,70} The room temperature values are 1.9×10^{-11} cm³/sec, 2.0×10^{-11} cm³/sec and 2.0×10^{-11} cm³/sec as obtained in references 61, 67 and 70, respectively.

The rate coefficients for the charge exchange of N^+ , N_4^+ and O^+ with H_2O have been measured⁶¹ recently, where the corresponding room temperature values are 2.8×10^{-9} cm³/sec, 3.0×10^{-9} cm³/sec and 3.2×10^{-9} cm³/sec, respectively. The charge exchange of N_2^+ with H_2O , however, has two channels⁶¹ resulting in H_2O^+ and N_2H^+ with a branching ratio of 0.82 and 0.18, respectively. As for N_3^+ , its reaction with H_2O yields⁶¹ H_2NO^+ .

The rate coefficient for the reaction of O^+ with N_2 to form NO^+ has been measured recently and the room temperature⁶¹ coefficient is 1.2×10^{-12} cm³/sec. This is in good agreement with previous measurement⁷¹ of the rate coefficient. However, the reaction O^+ with N_2 depends on both the vibrational temperature of the N_2 and on the kinetic^{67,71} temperature of the ion.

The rate coefficients for the preceding reactions are summarized in

Table V along with few pertinent switching and rearrangement processes.

Table V
Charge Exchange, Switching and Rearrangement Reaction Rate Coefficients

<u>Reaction</u>	<u>Coefficient (cm³/sec)</u> (T _a in eV)	<u>Reference</u>
N ⁺ + O ₂ → O ₂ ⁺ + N	3.4 × 10 ⁻¹⁰ T _a = 0.025	59
	3.1 × 10 ⁻¹⁰ T _a = 0.025	61
	2.8 × 10 ⁻¹⁰ T _a = 0.025 - 0.39	37,67
	5.3 × 10 ⁻¹⁰ (T _a) ^{.57} , T _a > 0.39	37,67
N ⁺ + O ₂ → NO ⁺ + O	3.1 × 10 ⁻¹⁰ , T _a = 0.025	59
	2.6 × 10 ⁻¹⁰ , T _a = 0.025	61
	2.8 × 10 ⁻¹⁰ , T _a = 0.025 - 0.39	37,67
	4.4 × 10 ⁻¹⁰ (T _a) ^{.57} , use is made of data from refs. 60 and 66	
N ⁺ + O ₂ → O ⁺ + NO	6.7 × 10 ⁻¹¹ , T _a = 0.025	59
	3.7 × 10 ⁻¹¹ , T _a = 0.025	61
N ₂ ⁺ + O ₂ → O ₂ ⁺ + N ₂	5.0 × 10 ⁻¹¹ , T _a = 0.025	67
	5.1 × 10 ⁻¹¹ , T _a = 0.025	61
	2.7 × 10 ⁻¹¹ (T _a) ^{-0.8} , T _a ≤ 0.3	67
	4.2 × 10 ⁻¹¹ (T _a) ^{1.4} , T _a > 0.3	67
N ₃ ⁺ + O ₂ $\begin{matrix} \text{a} \\ \text{b} \end{matrix}$ NO ⁺ + N ₂ + O	7.7 × 10 ⁻¹¹ , T _a = 0.025	59
	5.1 × 10 ⁻¹¹ , T _a = 0.025	61

Table V continued

<u>Reaction</u>	<u>Coefficient</u>	<u>Reference</u>
	7.5×10^{-13} , $0.025 T_a \leq .1$	67,70
	$3.2 \times 10^{-11} (T_a)^{1.38} T_a > 0.1$	
	$T_a = T_v$	
$O_4^+ + H_2O \rightarrow O_2^+ \cdot H_2O + O_2$	1.5×10^{-9} , $T_a = 0.025$	64
$O_2^+ \cdot H_2O + H_2O \xrightarrow{a} H_3O^+ \cdot OH + O_2$	1.2×10^{-9} , $T_a = 0.025$	64
	$a = 1.0 \times 10^{-9}$	
$\xrightarrow{b} H_3O^+ + OH + O_2$	$b = 2.0 \times 10^{-10}$, $T_a = 0.025$	
$H_3O^+ \cdot OH + H_2O \rightarrow H_3O^+ \cdot H_2O + OH$	1.4×10^{-9} , $T_a = 0.025$	64
$H_2O^+ + H_2O \rightarrow H_3O^+ + OH$	1.8×10^{-9} , $T_a = 0.025$	37
$H_2O^+ + O_2 \rightarrow O_2^+ + H_2O$	2.0×10^{-10} , $T_a = 0.025$	37
$O_2^+ \cdot N_2 + O_2 \rightarrow O_4^+ + N_2$	1.0×10^{-9} , $T_a = 0.025$	37
$O_2^+ \cdot N_2 + H_2O \rightarrow O_2^+ \cdot H_2O + N_2$	4.0×10^{-9} , $T_a = 0.025$	37

4.6 OTHER REACTIONS

In this section we discuss few other reactions whose rate coefficients are summarized in Table VI.

The three-body recombination of positive ions with the third body being an electron or a neutral (reactions 32, 33 and 34, 35, respectively) have not been studied extensively. The theoretical efforts have concentrated on hydrogen plasmas and are generally valid for low electron temperatures. However, theoretical expressions,³⁵ accurate to within a factor of 2 - 5 for these recombinations can be given and are listed in Table VI.

The mutual neutralization coefficients have been measured mainly³⁵ at room temperature and some over a limited temperature range.³⁵ Their values and their estimated temperature dependences are listed in Table VI. For

higher cluster ions, a recent measurement⁷² yields values which are lower by a factor of 2 compared to the previously accepted values.³⁶

The three-body attachment of the free electrons to O_2 to form O_2^- with the third body being O_2 , N_2 and H_2O have been measured⁷³ at room temperature. However, the attachment rate coefficient when $M = O_2$ have also been measured in the electron temperature range⁷³ of 300 - 600°K. As for the $M = H_2O$ the temperature range is even more limited⁷² ($T_e = 300 - 400^\circ K$).

Table VI
Recombination, Neutralization and Attachment Coefficients

Reactions	Coefficient* (T_e and T_a in eV)	Reference
$e + M + (A^+, A_2^+)$ → $(A, A_2) + M$	$5.9 \times 10^{-31} \left(\frac{1}{T_e}\right)^{2.5}$	36,37
$e + e + (A^+, A_2^+)$ → $e + (A, A_2)$	$4.3 \times 10^{-27} \left(\frac{1}{T_e}\right)^{4.5}$	36,37
$O^+ + O^- \rightarrow O + O$	$4.2 \times 10^{-8} [T_a]^{-0.5}$	36,37
$N^+ + O^- \rightarrow N + O$	$4.1 \times 10^{-8} [T_a]^{-0.5}$	36,37
$O_2^+ + O^- \rightarrow O_2 + O$	$1.6 \times 10^{-8} [T_a]^{-0.5}$	36,37
$O_2^+ + O_2^- \rightarrow O_2 + O_2$	$6.6 \times 10^{-8} [T_a]^{-0.5}$	36,37
$N_2^+ + O_2^- \rightarrow O_2 + N_2$	$2.53 \times 10^{-8} [T_a]^{-0.5}$	36,37
$X^+ + Y^- \rightarrow X + Y$	$1.6 \times 10^{-8} [T_a]^{-0.5}$	36,37
$X^+ + Y^- \rightarrow X + Y$	$9.5 \times 10^{-9} [T_a]^{-0.5}$	72
$A^+ + B^- + M \rightarrow$ $A + B + M$	$2.9 \times 10^{-29} [T_a]^{-2.5}$	36,37
$X^+ + Y^- + M \rightarrow X + Y + M$	$1.0 \times 10^{-29} [T_a]^{-2.5}$	36,37

* Two and three body coefficients are in units of cm^3/sec and cm^6/sec , respectively.

Table VI continued

<u>Reaction</u>	<u>Coefficient</u>	<u>Reference</u>
$e + O_2 + O_2 \rightarrow O_2^- + O_2$	$3.6 \times 10^{-31} \left(\frac{1}{T_e}\right) \text{ Exp } \left(-\frac{0.052}{T_e}\right)$	73
$e + O_2 + N_2 \rightarrow O_2^- + O_2$	1.0×10^{-31}	73
$e + O_2 + H_2O \rightarrow O_2^- + H_2O$	1.4×10^{-29}	
$e + O_2 \rightarrow O^- + O$	$1.5 (T_e)^{-1.0} \times 10^{-10} \text{ Exp } \left(-\frac{5}{T_e}\right)$	73

5. COMMENTS ON THE REACTION RATES AND SOME RECOMMENDATIONS

We have presented in section 4 the current status of the reaction rate coefficients pertinent to the modeling of the ionization and deionization phenomena in air. These rate coefficients, however, can be categorized as follows:

- a) Most of the reaction rate coefficients are measured at room temperature (0.025 eV) only.
- b) A small number of the reactions have no measured or calculated rate coefficients, even at room temperature. Their coefficients are thus estimated, based on similarity and educated guesses.
- c) Many of the reaction coefficients are measured as a function of the temperature of the reactant. However, the temperature range for these measurements is narrow and generally is limited to few times the room temperature.
- d) Few of the reaction coefficients are measured over a wider temperature range.

To model an air plasma of moderate to high temperature [$T_e \sim (1-2)$ eV, $T_a = 0.1 - 0.5$ eV], one must utilize the current reaction rates. In doing so, however, one extends the known low temperature dependence of the relevant coefficients to regions of higher temperatures. Such an extension is not always warranted or accurate. Furthermore, in cases where the energy deposited in air is high and results in the enhancement of the vibrational modes of air molecules and their ions, additional complications may arise. It is possible that many of the pertinent reactions will be affected by the

vibrational temperature in one way or another. Unfortunately, very little is known or has been measured under these conditions except for the following reaction:

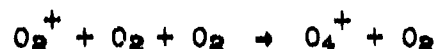
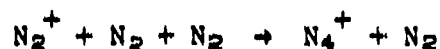


which is enhanced by a factor of ~ 40 , compared to the reaction at room temperature, when the vibrational temperature is (0.3 - 0.4 eV).

Clearly there is a need in extending the measurements of many of these reaction coefficients to moderate and higher temperatures. However, the following reactions merit immediate attentions.

A. ASSOCIATION REACTIONS:

The dependence of the following association reactions on the gas kinetic temperature is needed for T_g up to 0.1 eV.

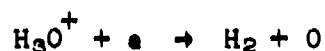
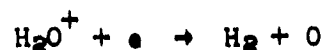


The reverse of these reactions, i.e. the collisional breakups are also needed and in the same temperature range. It is also of immediate interest to measure the association rates, when these molecules are vibrationally excited (T_v up to ~ 0.4 eV).

B. DISSOCIATIVE RECOMBINATIONS:

The rate coefficients for the following reactions and their dependence on the electron temperature is needed for T_e up to 1-2 eV.





The dissociative recombination of H_3O^+ has a large number of measurements and are carried out over a wide range of the electron and gas temperatures (see Table III section 4.3). The measurements of Hoppner, et al,⁴² at this juncture, present the most reasonable coefficient. However, a recent measurement⁴⁶ of the coefficient differs from Hoppner, et al,⁴² both in magnitude and the form of the temperature dependence. Thus it is of interest to delineate and clear up the controversy among these different measurements.^{42,46,47}

The dissociative recombination of NO^+ (see Table I section 4.1) has been measured by three different experimental techniques.³¹⁻³³ They predict the following temperature dependencies, $T_e^{-0.37}$, $T_e^{-0.83}$ and $T_e^{-0.5}$ which are obviously different. In addition to the experimental efforts, the dissociative recombination of NO^+ has also been investigated theoretically.⁷⁵⁻⁷⁸ There is some agreement on the theoretical behavior of the coefficient in the low and high electron temperature regimes. However, there is no agreement on the magnitude of the coefficient especially on the dissociation recombination of the vibrationally excited NO^+ . Therefore, it is of interest to delineate the problems associated with the dissociative recombination of NO^+ .

Under this category we include the need for extending the measurements of the dissociative recombination coefficients of the positive ion clusters to higher electron temperatures ($T_e > 0.06$ eV).

C. ELECTRIC FIELD DETACHMENT OF THE NEGATIVE IONS

It is of interest to know the detachment rates of negative ions (O^- , O_2^- clusters) under the influence of high electric fields.

REFERENCES

1. H. A. Bethe and A. J. Ashkin in "Experimental Nuclear Physics", Vol 1, E. Segre, Ed., John Wiley, (1953) New York.
2. A. Dalgarno, in "Atomic and Molecular Processes", Bates, Ed. Academic (1962) New York.
3. R. M. Sternheimer, Phys. Rev. 145, 247 (1966), R. M. Sternheimer and R. F. Peierls, Phys. Rev. B3, 3681 (1971).
4. L. Pages, E. Bertel, H. Joffre and L. Sklavenites, Atomic Data 4, 1, (1972).
5. W. Heitler, "The Quantum Theory of Radiation", 3rd Ed. Oxford (1954).
6. H. W. Koch and J. W. Motz, Rev. Mod Phys. 31, 920 (1959).
7. S. C. Brown in "Encyclopedia of Physics", S. Flugge, Ed. Vol XXII Springer Verlag, (1956) Berlin.
8. D. A. Hammer, K. A. Gerber and A. W. Ali, IEEE Trans. P.S. PS7, 8, (1979).
9. E. J. Lauer, R. J. Briggs, T. J. Fessenden, R. E. Hester and E. P. Lee, Physics of Fluids 21, 1344 (1978).
10. See e.g. F. W. Chambers, Phys Fluids 22, 483 (1979).
11. D. A. McArthur and J. W. Poukey, "Interaction of Relativistic Electron Beam with Neutral Gas", Sandia Laboratories Report SC-RR-72 0874 (1973).
12. U. Fano, Phys Rev. 92, 328 (1953).
13. L. V. Spencer and U. Fano, Phys. Rev. 93, 1172 (1954).
14. R. S. Stolarski and A. E. S. Green, J. Geophys. Res. 72, 3967 (1967).
15. R. Stolarski, Planet. Space Sci. 16, 1265 (1968).
16. B. C. Edgar, W. T. Miles and A. E. S. Green, J. Geophys. Res. 78, 6595 (1973).
17. P. M. Banks, C. R. Chappell, A. F. Nagy, J. Geophys Res. 79, 1459 (1974).
18. D. Strickland, P. C. Kepple, NRL Memo Report 2779 (1974).
19. L. G. Peterson, Phys., Rev. 187, 105 (1969).
20. T. E. Cravens, G. A. Victor and A. Dalgarno, Planet. Space Sci 23, 1059 (1975).
21. J. L. Fox, A. Dalgarno and A. Victor, Planet. Space Sci 25, 71 (1977).
22. J. Nishimura in "Handbuck der Physik", Vol XLVI/2, S. Flugge Ed., Springer Verlag (1967) Berlin.
23. R. D. Evans, "The Atomic Nucleus", McGraw-Hill, New York (1955).
24. P. Auger, J. Phys. Radium 6, 205 (1925);

25. R. W. Fink, R. C. Japson, H. Mark and C. D. Swift, Rev. Mod. Phys. 38, 513 (1966).
26. R. S. Narcisi and A. D. Bailey, J. Geophys. Res. 70, 3687 (1965).
27. F. C. Fehsenfeld and E. E. Ferguson, J. Geophys. Res. 70, 3687 (1965).
28. A. Good, D. A. Durden and P. Kebarle, J. Chem. Phys. 52, 222 (1970).
29. A. W. Ali, "Excitation and Ionization Cross Sections for Electron Beam and Microwave Energy Deposition in Air", NRL Memo Report (in press).
30. F. J. Mehr and M. A. Biondi, Phys Rev 181, 264 (1969) and references therein.
31. C. M. Huang, M. A. Biondi and R. Johnson, Phys. Rev. A 11, 901 (1975).
32. F. L. Walls, and G. H. Dunn, J. Geophys. Res. 70, 1911 (1974).
33. P. M. Mul and J. Wm. McGowan, J. Phys. B. Atom Molec. Phys. 12, 1591 (1979).
34. W. H. Kasner, and M. A. Biondi, Phys. Rev. 137, A317 (1965).
35. R. Hackman, Planet. Space Sci. 13, 667 (1965).
36. M. A. Biondi, Chapter 16 Defense Nuclear Agency Reaction Rate Handbook DNA 1948H, Bortner and Bauer Eds. published by DASIAC, DOD Nuclear Information and Analysis Center GE-Tempo, Santa Barbara, CA (1974).
37. T. Bauer and M. H. Bortner, Chapter 24, Defense Nuclear Agency Reaction Rate Handbook DNA 1948 H, Bortner and Bauer Eds. published by DASIAC, DOD Nuclear Information and Analysis Center GE-Tempo, Santa Barbara, CA (1974).
38. W. H. Kasner, and M. A. Biondi, Phys. Rev. 174, 139 (1968).
39. I. C. Plumb, D. Smith and N. G. Adams, J. Phys. B, Atom Molec. Phys. 5, 1762 (1972).
40. Estimated as similar to that of $\text{NO}^+ \cdot \text{N}_2$ see e.g. Ref. 37.
41. M. T. Leu, M. A. Biondi and R. Johnson, Phys. Rev. A 1, 292 (1973).
42. R. A. Heppner, F. L. Walls, W. T. Armstrong and G. H. Dunn, Phys. Rev. A. 13, 1000 (1976).
43. J. A. Green and T. M. Sugden, Ninth Symposium on Combustion (Combustion Institute, Pittsburg, Pa. 1963) p 607.
44. L. N. Wilson and E. W. Evans, J. Chem. Phys. 46, 859 (1967).
45. W. Lindinger, Phys. Rev. A 7, 328 (1973).
46. G. L. Ogram, Jen-Shih Chang and R. M. Hobson, Phys. Rev. A 21, 982 (1980).

47. J. Wm. McGowan, P. M. Mul., V. S. D'Angelo, J. B. A. Mitchel, P. DeFrance and H. R. Froelich, Phys. Rev. Lett. 42, 373 (1979).
48. D. L. Albritton, Atomic Data and Nuclear Data Tables. 22, 1 (1978).
49. R. N. Varney, Phys. Rev. 174, 165 (1968).
50. R. N. Varney, J. Geophys. 72, 5578 (1967).
51. R. N. Varney, Phys. Rev. 89, 708 (1953).
52. R. N. Varney, J. Chem. Phys. 31, 1314 (1959).
53. J. K. Vogel, Z. Physik 148, 355 (1957).
54. P. Warneck, J. Chem. Phys. 46, 502 (1967).
55. L. G. McNight, K. B. AcAfee and D. Sipler, Phys. Rev. 164, 62 (1967).
56. S. B. Woo, J. Chem. Phys. 42, 1251 (1965).
57. A. Good, D. A. Durden and P. Kebarle, J. Chem. Phys. 52, 212 (1970).
58. J. D. Payzant and P. Kebarle, J. Chem. Phys. 53, 4723 (1970).
59. J. L. McCrumb and P. Warneck, J. Chem. Phys. 66, 5416 (1977).
60. T. D. Mark, Int. J. Mass Spectrom., Ion Phys. 9, 387 (1972) and references therein.
61. D. Smith, N. G. Adams and T. M. Miller, J. Chem. Phys. 69, 308 (1978).
62. F. E. Niles BRL Report No. 1702, U.S. Ballistic Research Laboratories, Aberdeen, MD. (1974).
63. J. T. Mosely, R. M. Snuggs, D. W. Martin and E. W. McDaniel, Phys. Rev. 178, 240 (1969).
64. C. J. Howard, V. M. Bierbaum, H. W. Rundle and F. Kaufman, J. Chem. Phys. 57, 3491 (1972).
65. D. J. Payzant, A. J. Cunningham and P. Kebarle, J. Chem. Phys. 59, 5615 (1973).
66. F. C. Fehsenfeld, M. Mosesman and E. E. Ferguson, J. Chem. Phys. 55, 2215 (1971).
67. H. McFarland, D. L. Albritton, F. C. Fehsenfeld, E. E. Ferguson and A. L. Achmeltekopf, J. Chem. Phys. 59, 6620 (1973).
68. W. Lindinger, J. Chem. Phys. 64, 3720 (1976).
69. W. Lindinger, I. Dotan, D. L. Albritton and F. C. Fehsenfeld, J. Chem. Phys. 68, 2607 (1978).
70. R. Johnsen and M. A. Biondi, J. Chem. Phys. 59, 3504 (1973).
71. A. L. Schemeltekopf, E. E. Ferguson and F. C. Fehsenfeld, J. Chem. Phys. 48, 2966 (1968) and references therein.

72. D. Smith, N. G. Adams and M. J. Church, Planet Space Sci. 24, 697 (1976).
73. A. V. Phelps, Chapter 17 DNA Reaction Rate Handbook DNA 1948 H, Bortner and Bauer, Eds. published by DASIAC, DOD Nuclear Information and Analysis Center GE-Tempo, Santa Barbra, CA. (1972).
74. The cross section of D. Rapp and D. D. Brigalia, J. Chem. Phys. 43, 1480 (1965) was averaged over a Maxwellian velocity distribution to obtain an approximate rate coefficient.
75. T. F. O'Malley, Phys. Rev. 185, 101 (1969).
76. J. N. Bardsley and M. A. Biondi in "Advances in Atomic and Molecular Physics", Bates and Bederson Eds. volume 6, 1 (1970), and references therein.
77. H. H. Michels, "Theoretical Studies of Dissociative Recombination Kinetics", Air Force Weapons Laboratory Report ARWL-TR 73-288, (1974).
78. C. M. Lee, Phys. Rev. 16, 109 (1977).

DISTRIBUTION LIST

Commander
Naval Sea Systems Command
Department of the Navy
Washington, D.C. 20363
ATTN: NAVSEA O3H (Dr. C. F. Sharn)

Central Intelligence Agency
P.O. Box 1925
Washington, D.C. 20013
ATTN: Dr. C. Miller/OSI

Air Force Weapons Laboratory
Kirtland Air Force Base
Albuquerque, New Mexico 87117

U.S. Army Ballistics Research Laboratory
Aberdeen Proving Ground, Maryland 21005
ATTN: Dr. D. Eccleshall (DRXBR-BM)

Ballistic Missile Defense Advanced Technology Center
P.O. Box 1500
Huntsville, Alabama 35807
ATTN: Dr. L. Harvard (BMDSATC-1)

B-K Dynamics Inc.
15825 Shady Grove Road
Rockville, Maryland 20850
ATTN: Mr. I. Kuhn

Lawrence Livermore Laboratory
University of California
Livermore, California 94550
ATTN: Dr. R.J. Briggs
Dr. T. Fessenden
Dr. E.P. Lee

Mission Research Corporation
735 State Street
Santa Barbara, California 93102
ATTN: Dr. C. Longmire
Dr. N. Carron

National Bureau of Standards
Gaithersburg, Maryland 20760
ATTN: Dr. Mark Wilson

Science Applications, Inc.
Security Office
5 Palo Alto Square, Suite 200
Palo Alto, California 94304
ATTN: Dr. R.R. Johnston
Dr. Leon Feinstein

Naval Surface Weapons Center
White Oak Laboratory
Silver Spring, Maryland 20910

ATTN: Mr. R.J. Biegalski
Dr. R. Cawley
Dr. J.W. Forbes
Dr. D.L. Love
Dr. C.M. Huddleston
Mr. W.M. Kinckley
Dr. G.E. Hudson
Mr. G.J. Peters
Mr. N.E. Scofield
Dr. E.C. Whitman
Dr. M.H. Cha
Dr. H.S. Uhm
Dr. R.B. Fiorito

C.S. Draper Laboratories
Cambridge, Massachusetts 02139

ATTN: Dr. E. Olsson
Dr. I. Matson

Physical Dynamics, Inc.
P.O. Box 1883
Lajolla, California 92038

Office of Naval Research
Department of the Navy
Arlington, Virginia 22217

ATTN: Dr. W.J. Condell (Code 421)
Dr. T. Berlincourt (Code 464)

Avco Everett Research Laboratory
2385 Revere Beach Pkwy.
Everett, Massachusetts 02149

ATTN: Dr. R. Patrick
Dr. Dennis Reilly

Defense Technical Information Center
Cameron Station
5010 Duke Street
Alexandria, VA 22314 (12 copies)

Naval Research Laboratory
Washington, D.C. 20375

ATTN: M. Lampe - Code 4792
M. Friedman - Code 4700.1
J.R. Greig - Code 4763 (1 copy)
I.M. Vitkovitsky - Code 4770
T. Coffey - Code 4000
Superintendent, Plasma Physics Division - Code 4700 (26 copies)
Library - Code 2626 (20 copies)
A. Ali - Code 4700.1T (25 copies)
J. Brown

Defense Advanced Research Projects Agency
1400 Wilson Blvd.
Arlington, Virginia 22209
ATTN: Dr. J. Mangano
Dr. J. Bayless

JAYCOR
205 S. Whiting St.
Alexandria, Virginia 22304
ATTN: Drs. D. Tidman
R. Hubbard
J. Gillory

JAYCOR
Naval Research Laboratory
Washington, D.C. 20375
ATTN: Dr. R. Fensler - Code 4770

Mission Research Corp.
1400 San Mateo, S.E.
Albuquerque, NM 87108
ATTN: Dr. Brendan Godfrey

Princeton University
Plasma Physica Laboratory
Princeton, NJ 08540
ATTN: Dr. F. Perkins, Jr.

McDonnell Douglas Research Laboratories
Dept. 223, Bldg, 33, Level 45
Box 516
St. Louis, MO 63166
ATTN: Dr. Michael Greenspan

Cornell University
Ithaca, NY 14853
ATTN: Prof. David Hammer

Sandia Laboratories
Albuquerque, NM 87135
ATTN: Dr. Bruce Miller
Dr. Barbara Epstein
Dr. John Olsen
Dr. Don Cook

Naval Air Systems Command
Washington, D.C. 20361
ATTN: Dr. R.J. Wasneski, Code AIR-350F

Beers Associates, Inc.
P.O. Box 2549
Reston, VA 22090
ATTN: Dr. Douglas Strickland

R and D Associates
P.O. Box 9695
Marina del Rey, California 90291
ATTN: Dr. F. Gilmore

Director
Defense Nuclear Agency
Washington, D.C. 20305
ATTN: Dr. C. Fitz (RAAE)
Dr. P. Lunn (RAAE)